

Electrically Controlled Localized Charge Trapping at Amorphous Fluoropolymer–Electrolyte Interfaces

Hao Wu,* Ranabir Dey, Igor Siretanu, Dirk van den Ende, Lingling Shui, Guofu Zhou, and Frieder Mugele*

Charge trapping is a long-standing problem in electrowetting on dielectric, causing reliability reduction and restricting its practical applications. Although this phenomenon is investigated macroscopically, the microscopic investigations are still lacking. In this work, the trapped charges are proven to be localized at the three-phase contact line (TPCL) region by using three detecting methods—local contact angle measurements, electrowetting (EW) probe, and Kelvin probe force microscopy. Moreover, it is demonstrated that this EW-assisted charge injection (EWCI) process can be utilized as a simple and low-cost method to deposit charges on fluoropolymer surfaces. Charge densities near the TPCL up to 0.46 mC m^{-2} and line widths of the deposited charge ranging from 20 to 300 μm are achieved by the proposed EWCI method. Particularly, negative charge densities do not degrade even after a “harsh” testing with a water droplet on top of the sample surfaces for 12 h, as well as after being treated by water vapor for 3 h. These findings provide an approach for applications which desire stable and controllable surface charges.

1. Introduction

Amorphous fluoropolymers (AFPs) are popular materials for various applications^[1–5] because of the unique combination of favorable material properties such as chemical inertness, mechanical strength, water repellency, dielectric strength, optical transparency, and easy solution processability.^[5,6] For these reasons, AFPs are also predominantly used as insulating and hydrophobic layer in electrowetting (EW) devices.^[6–11] EW, which is often also denoted as “electrowetting on dielectric” (EWOD) to emphasize the relevance of the dielectric layer, relies on the fact that ionic charge carriers have in general a rather low affinity to the weakly polarizable AFPs. However, at the same time, fluoropolymers have been

used for decades as charge storage (electret) materials with applications in electro-mechanical transductions, such as microphones, micro-electro-mechanical systems, and electric generators.^[12–14] These applications rely on the fact that charges, once deposited on or within AFPs, remain stable in the materials. The purpose of the present work is to shed light on these two contradictory aspects of charge repellence and charge storage in AFPs that together control the extent of charge injection into AFPs during EWOD at high voltage. Such EW-assisted charge injection (EWCI), if done in a controllable way, can be used as an innovative method for generating permanent charge patterns on AFPs.

The reliability of any EW applications in microfluidics,^[15,16] optofluidics,^[17,18] display technology,^[19,20] and energy harvesting^[21] relies on the reproducibility, performance, and durability of the dielectric layer, and hence, the stability of AFPs is particularly important.^[22–25] Charge trapping at the dielectric/electrolyte interfaces is a long-standing problem in EW, leading to the degradation of the electrical response of AFP films, and thus causing the contact angle (CA) saturation and failures in EWOD devices.^[21,26,27] While early experiments with composite dielectrics displayed a reversible response and symmetric saturation for positive and negative bias voltage, suggesting substantial mobility of both types of charge carriers upon injection into the AFP films,^[28] more recent studies displayed a strongly asymmetric and sometimes irreversible response.^[29,30] It was also reported that AFP materials even spontaneously assumed a permanent negative surface charge upon extended

H. Wu, Prof. L. Shui, Prof. G. Zhou
Guangdong Provincial Key Laboratory of Optical Information
Materials and Technology & Institute of Electronic Paper Displays
South China Academy of Advanced Optoelectronics
South China Normal University
Guangzhou 510006, P. R. China

H. Wu, Prof. L. Shui, Prof. G. Zhou
National Center for International Research on Green Optoelectronics
South China Normal University
Guangzhou 510006, P. R. China

H. Wu, Dr. R. Dey, Dr. I. Siretanu, Dr. D. van den Ende, Prof. F. Mugele
Physics of Complex Fluids
Faculty of Science and Technology
MESA+ Institute for Nanotechnology
University of Twente
Enschede 7500AE, the Netherlands
E-mail: hao.wu@utwente.nl; f.mugele@utwente.nl

Dr. R. Dey
Dynamics of Complex Fluids
Max Planck Institute for Dynamics and Self-organization
Am Fassberg 17, Goettingen 37077, Germany

Prof. G. Zhou
Shenzhen Guohua Optoelectronics Tech. Co. Ltd.
Shenzhen 518110, P. R. China

 The ORCID identification number(s) for the author(s) of this article can be found under <https://doi.org/10.1002/smll.201905726>.

© 2019 The Authors. Published by WILEY-VCH Verlag GmbH & Co. KGaA, Weinheim. This is an open access article under the terms of the Creative Commons Attribution License, which permits use, distribution and reproduction in any medium, provided the original work is properly cited.

DOI: 10.1002/smll.201905726

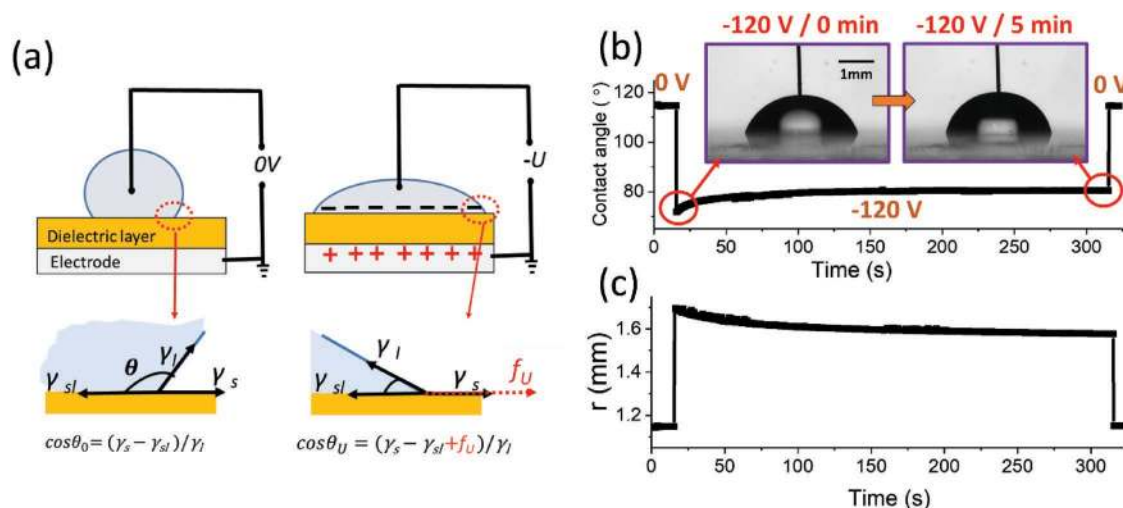


Figure 1. a) Illustration of the EW on dielectric (EWOD) principle. γ_s , γ_l , and γ_{sl} are the solid/air, liquid/air, and solid/liquid interface tensions. f_U is a pulling force under the applied voltage of U . b) Water/air CA and c) contact line radius (r) of a 5 μ L water droplet depending on time with -120 V voltage applied. Insets of (b) show side view images of charging droplets immediately after applying the voltage and after 5 min. This charging process is shown in Video S1 in the Supporting Information.

(several hours) contacting with water in the absence of any applied voltage.^[31]

Since most studies on EW-induced charge trapping phenomena mainly focus on the response of the macroscopic CAs and the total electrical currents, there is a significant lack of a quantitative description of the underlying microscopic charge trapping phenomenon. Moreover, a clear understanding of the correlation between the charge trapping and the macroscopic wetting characteristics has still remained elusive. It was recognized that diverging electric fields in the vicinity of the three-phase contact line (TPCL) cause various types of nonlinear response of the materials during EW, which may limit the minimum CA.^[32,33] However, whether the heterogeneity of the electric field actually leads to the charge trapping and induces permanent changes in the local surfaces of AFPs is still unclear. The charge injection process was assumed to essentially follow the distribution of the electric field with its well-established divergence near the TPCL.^[34,35] However, several recent studies on charge injection during EWOD using local surface potential measurement with noncontact electrostatic probes show otherwise.^[27,36,37] Surprisingly, the measured surface potential distributions were reported to be rather broad with a maximum in the center of the droplet, thereby challenging the classical view based on the local field divergence.^[27,36,37]

In this work, we analyze the charge distribution generated on the Teflon AF (a typical AFP material) surfaces by EW at high voltage with unprecedented lateral resolution, and explore the usage of the EWCI method for localized charge deposition at AFP surfaces. Three complementary techniques are used to reveal the local charge distribution on single-layer AFP surfaces. We quantitatively demonstrate that EW-induced charge injection via a water drop is highly localized. Based on this, a simple and low-cost approach is proposed and validated to generate stable charge patterns with controllable line width and charge density. As a result, we can tune the surface properties of AFP by EWCI at a microscale level without complex microfabrication processes involving high-end instruments. The excellent

stability of the negative trapping charges, in particular in a “harsh” environment under water or high humidity, demonstrates the potential of the proposed methodology for a wide range of applications requiring stable surface charges.^[38–42]

2. Results and Discussion

2.1. Evidence of Charge Trapping Phenomenon

2.1.1. Macroscopic Surface Wettability upon Charging

The working principle of EWOD is schematically shown in Figure 1a. When a voltage (U) is applied on the dielectric layer via an electrolyte droplet and the bottom electrode, a pulling force (f_U) derived from the applied electric field pulls the TPCL toward the outside direction of the droplet, and thus changes the CA. This pulling force $f_U = \frac{\sigma_s^2}{2c}$ is governed by the total amount of charges at the electrolyte/solid interfaces σ_s (the same amount of counter charges are in the bottom electrode) and the capacitance per unit area of the dielectric layer (c). When U is relatively low, there is no “trapping charge” at the electrolyte/solid interfaces. All surface charges are supposed to be contributed by the electric field, and the pulling force is $f_U = \frac{1}{2}cU^2$. Thus, the CA $\theta(U)$ is given by the classical Young–Lippmann EW model

$$\cos\theta(U) = \cos\theta_Y + \frac{c}{2\gamma}U^2 \quad (1)$$

where θ_Y is Young’s angle, γ is the surface tension of the liquid, and U is the applied voltage. The CA response under the applied voltage is shown in Figure S1 in the Supporting Information. However, when the voltage reaches a certain high

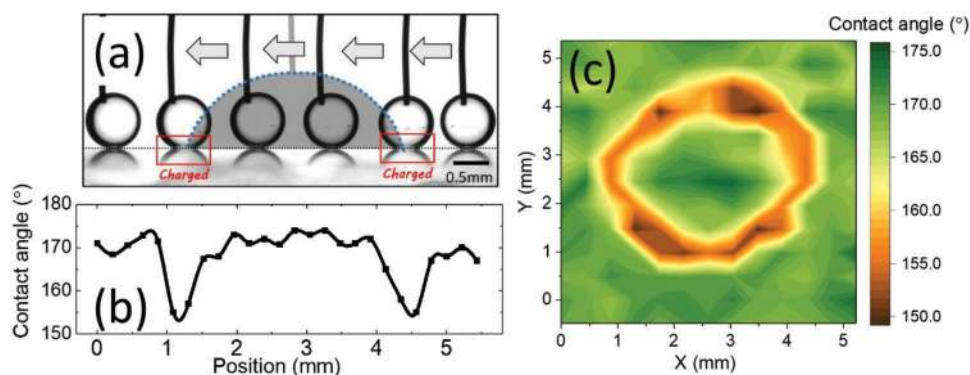


Figure 2. CA reduction along contact line of charging drop. a) Snapshots of electrically grounded probe droplets ($V = 0.3 \mu\text{L}$) at different locations relative to the original charging droplet (gray background; $V = 5 \mu\text{L}$) that was used to charge the surface ($U_c = -120 \text{ V}$; $t_c = 5 \text{ min}$). This test is also shown in Video S2 in the Supporting Information. b) CA $\theta(U = 0)$ of electrically grounded drop versus position extracted from (a). c) 2D map of $\theta(U = 0)$ (12×13 locations) as measured by probe drop.

value, charges can be trapped at the electrolyte/solid interfaces, thus causing CA saturation.^[28] The charge trapping process could be reversible or irreversible. Once the charges are irreversibly trapped in the dielectric layer, the electric response of the dielectric layer will be permanently degraded.^[21,30]

To investigate the charge trapping phenomenon in EWOD, we intentionally achieve the CA saturation by abruptly applying a voltage as high as -120 V to the EWOD system. As a response, the drop spreads within a few tens of ms from the initial CA of $\approx 115^\circ$ to $\approx 70^\circ$ (Figure 1b). Subsequently, a slow relaxation to $\theta(U_c) \approx 80^\circ$ takes place for approximately 1 min. Along with the increase in CA, the radius of footprint area of the drop decreases (Figure 1c). This macroscopic CA retreat phenomenon has also been observed in previous works.^[23,29,36] Because of the humid environment, we know that this relaxation is not caused by evaporation (Figure S2, Supporting Information). After 300 s, when the charging voltage is turned off, subsequent inspection of the samples by optical and by atomic force microscopy (AFM) does not display any appreciable variation of the surface topography.

As discussed above, the CA variation in EW is the joint effect of the materials' surface (interface) tension, the applied voltage, the reversible, and the irreversible trapping charges. In the present experiment, the material surface (interface) tension and the applied voltage ($U = -120 \text{ V}$) are kept constant, and the pulling force contributed by the applied voltage is $f_U = \frac{1}{2} c U^2 = 158 \text{ mN m}^{-1}$. Due to the effect of trapping charges, the pulling forces are suppressed to $\gamma_{w/a} (\cos 115^\circ - \cos 70^\circ) = 55 \text{ mN m}^{-1}$ for the initial CA of 70° to $\gamma_{w/a} (\cos 115^\circ - \cos 80^\circ) = 43 \text{ mN m}^{-1}$ for the final CA of 80° (water/air interfacial tension $\gamma_{w/a} = 72 \text{ mN m}^{-1}$). The 12 mN m^{-1} reduction of pulling force is supposed to be caused by the charge density variation of both reversible and irreversible charge trapping during this charging process.

2.1.2. Local CAs

To further investigate whether the charge trapping is reversible and occurs over the entire drop–substrate interface, we remove

the charging drop (after turning off the charging voltage) and subsequently investigate the surface properties in several manners. First, the wettability of the surface is investigated with high lateral resolution using a CA measurement with a much smaller probe droplet ($0.3 \mu\text{L}$) (the setup shown in Figure S3, Supporting Information). To minimize disturbing effects of CA hysteresis, these measurements are carried out in ambient oil. **Figure 2a** shows a composite side view image of such a probe droplet at various locations on the surface. Video S2 in the Supporting Information shows the process of this local CA measurement. The probe drop is always in contact with the electrically grounded Pt wire, guaranteeing zero potential drop between the drop and the electrode on the substrate. **Figure 2b** shows a 1D variation of $\theta(U = 0)$ with position along a diameter of the charging droplet footprint; **Figure 2c** shows a full 2D map of the reduction of $\theta(U = 0)$ all along the contact line of the original charging drop. Away from the position of the charging drop, the CA of the probe drop is close to 170° . In the center of the charging drop, the same CA is observed within the resolution of this measurement. In contrast, in the region close to the contact line during charging, $\theta(U = 0)$ is reduced to about 155° . The width of this region with reduced CA is approximately $0.2\text{--}0.5 \text{ mm}$. The variation of the CA corresponds to a pulling force of $-\Delta f_o = \gamma_{w/o} (\cos 155^\circ - \cos 170^\circ) = 0.08 \gamma_{w/o} \approx 3.2 \text{ mN m}^{-1}$ (water/oil interfacial tension $\gamma_{w/o} = 41 \text{ mJ m}^{-2}$). Assuming Δf_o is contributed by the trapped charges $-\Delta f_o = \sigma_T^2/2c$, the surface charge density can be estimate to be around 0.37 mC m^{-2} .

2.1.3. EW Response

With the trapping charges existing on a dielectric surface, the EW response curves follow a modified EW equation^[28,31] of

$$\cos \theta(U) = \cos \theta_Y + \frac{c}{2\gamma} (U - U_T)^2 \quad (2)$$

where U_T is denoted as the “trapping” voltage, corresponds to the potential on the droplet when it contains zero charge (i.e., all the counter charges induced by the trapping charges are

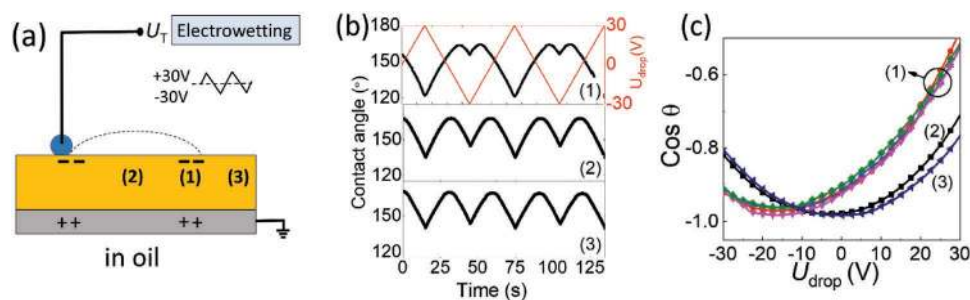


Figure 3. a) Schematic of measuring trapping charge by EW probe with different probing regions: 1) contact line; 2) drop center; 3) pristine surface. The dashed line represents the shape profile of the previous electrolyte drop used during the EWCI process. This drop was removed immediately after the EWCI process. b) EW response curves and c) CA versus applied voltage (U_{drop}) of all three regions. (charging conditions: -120 V for 5 min).

remained in the bottom electrode). The observation of a finite offset voltage U_T directly points to the presence of a finite permanent surface charge density of

$$\sigma_T = c U_T \quad (3)$$

at the polymer–electrolyte interfaces.^[28,31]

The reduction of $\theta(U = 0)$ presented in Figure 2 alone does not clearly indicate whether the effect is caused by local chemical variation of the surface along the contact line, which would reduce Young's angle θ_y , or whether it is indeed caused by the expected injection of surface charge, which would give rise to a finite value of trapping voltage U_T . To distinguish between the two scenarios, we perform EW measurements using probe droplets ($0.5 \mu\text{L}$). The asymmetry of EW curve is found to be strongly position-dependent on the surface, being much more pronounced close to the contact line during charging, Region 2 in Figure 3, as compared to the central part of the charging drop (Region 1). Fitting the Equation (2) to the data shown in Figure 3c, the trapping voltages are $U_T(1) = -16$ V, $U_T(2) = -3$ V, and $U_T(3) = -1$ V in Regions 1, 2, and 3, respectively. The calculated σ_T according to Equation (3) are 0.34 , 0.06 , and 0.02 mC m^{-2} in Regions 1, 2, and 3, respectively. σ_T of 0.34 mC m^{-2} at Region 1 is consistent with the calculated values from the local CA $\theta(U = 0)$ variation in Figure 2, which is 0.37 mC m^{-2} . The consistency of σ_T value calculated from these two methods indicates that the reduction of $\theta(U = 0)$ in Figure 2 is indeed induced by the irreversible charge trapping, instead of the chemical surface modification. Hence, the AFP surface modification is caused by the deposition of charges during EW rather than by any chemical modification.

2.1.4. Kelvin Probe Force Microscopy (KPFM) Measurement

Considering the fact that the probe droplets spread upon applying the voltage, and thus their footprint area increases quickly, one may wonder whether the probe drop remains within the narrow ring around the original contact line where the deposited charges are presumably trapped. If the probe drop spreads beyond the charging area, the measured asymmetry of the EW response and the value of U_T would in part reflect the finite lateral extent of the deposited charge pattern rather than its absolute value.

To overcome the resolution limitation of CA-based detecting method, we performed AFM and KPFM measurements on the prepared charged Teflon surfaces in ambient air after removing the charging drop without immersing the surface into oil. The sample is charged by -90 V for 5 min. The AFM topography images display a very smooth surface with a roughness of a few nanometers. No indications of topographic surface modifications due to the charging process could be identified. In contrast, the KPFM measurements indeed reveal strong lateral variations of the surface potential U_S in the region of the contact line, as shown in Figure 4. Overall, the KPFM measurements confirm the important observations of the macroscopic surface characterization (Figures 2 and 3). U_S is essentially constant and small in the center of the charging drop–substrate interface. Pronounced variations of U_S occur in the rim along the contact line of the original charging drop. This rim is around $200\text{--}300 \mu\text{m}$ wide, only slightly smaller than that suggested by the CA and EW response measurements. The absolute value of the local surface potential in the KPFM measurements is around -10 V

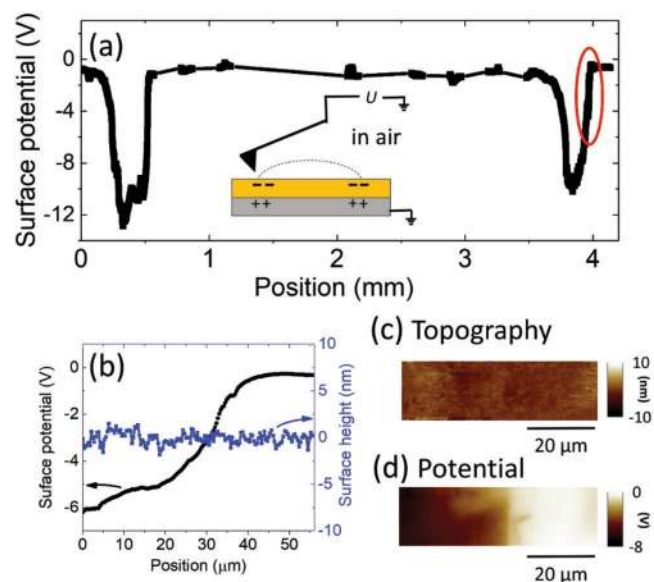


Figure 4. a) Surface potential map measured by stitching several KPFM measurements of $90 \times 90 \mu\text{m}^2$ (charging conditions: -90 V for 5 min). b) Comparison of surface potential (black) and surface height (blue) in the region highlighted on the right in (a). c) The surface topography and d) local surface potential U_S in the same region as in (b).

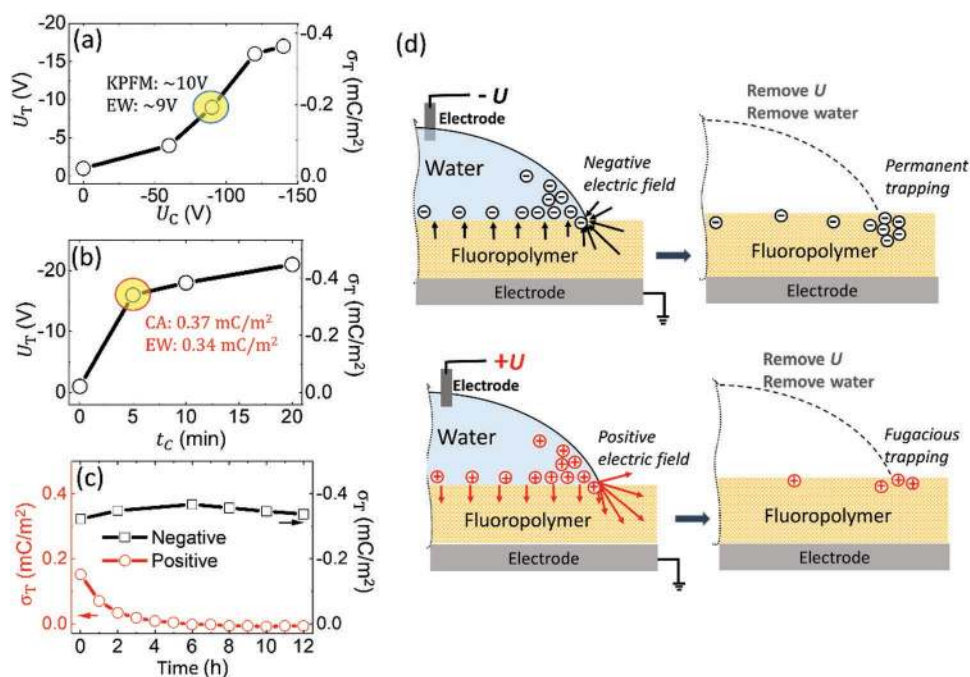


Figure 5. Trapping voltage U_T and trapped charge density σ_T based on EW measurements as a function of a) charging voltage (U_C) at fixed charging time ($t_C = 5$ min) and b) changing time (t_C) at fixed charging voltage ($U_C = -120$ V). Comparison of U_T and σ_T measured by EW, KPFM, and local CA of the samples charged at the same conditions is highlighted in (a) and (b). c) Comparison of the trapping charge density as a function of time (30 V amplitude, 60 s period; continuous measurement) between samples charged by -120 V (black) and $+120$ V (red). The EW curves for (a) and (b), and the corresponding U_T information for (c) are shown in Figure S5 in the Supporting Information. d) Illustration of charge trapping process at Teflon surface. The black and red arrows indicate the electric field.

which is consistent with the EW-response measurements at the same charging conditions (shown in Figure 5a and Figure S5, Supporting Information). Nano-sized KPFM probe in ambient air and macroscopic EW-probed drops in ambient oil thus experience the same surface charge density σ_T , which could be obtained from the measured voltages using Equation (3) with $U_T = U_S$ (the detailed calculation of detecting surface potential U_S and trapping voltage U_T by KPFM can be found in the Supporting Information and Figure S4, Supporting Information). Thus far, these results from three types of micro- and nanoscale measurements reveal and confirm that the charges are indeed trapped at the AFP surfaces after EW process and accumulate at the TPCL regions. These results also indicate that for EW applications driven by DC voltage, failures such as charge trapping or film break-down are more likely to occur at the TPCL region. Consequently, protecting the TPCL region may help to improve the quality and reliability of such EW devices.

2.2. Controlling Charge Trapping by EWCI

Having established and quantitatively characterized EWCI, we proceed to explore how to control density and distribution of the injected charge by our approach can lead to a novel, simple, and low-cost method of printing controllable surface charges. Such controllable surface charges are favored in many studies, such as energy harvesting,^[38,43,44] super capacitors,^[45,46] transport of droplets,^[42] nanofluidics or nanoparticles,^[47,48] water deionization,^[49] antifouling,^[50] and protein adsorption.^[51]

2.2.1. Controlling the Maximum Charge Density

To optimize the local surface charge density within the rim, we vary the applied voltage and duration for injecting charges, as well as the polarity of the voltage (Figure 5 and Figure S5, Supporting Information). For a fixed charging time of 5 min, the highest charge density of 0.37 mC m^{-2} is achieved at the highest negative charging voltage of -140 V (the application of higher voltages is hampered by risk of dielectric breakdown. The dielectric strength of the dielectric films is shown in Figure S6, Supporting Information). For a safe charging voltage of -120 V, the highest charge density as obtained approaching $\sigma_{\text{max}} = -0.46 \text{ mC m}^{-2}$ after 20 min. These results indicate that ten times higher charge density than that of the spontaneous charges^[31] is reached, and almost hundred times faster than that from spontaneous charge accumulation at Teflon AF surfaces in contact with water.^[31] This demonstrates the power of electric fields in immobilizing charge carriers at Teflon–water interfaces.

Negative charges deposited on the surface are very stable. No appreciable signs of degradation are observed even after 12 h of “harsh” testing by continuous probing with a water drop on top of the surface with trapping charges (Figure 5c). After 36 h of immersion in oil, the measured negative charge density is still not altered. We also exposed the charged AFP films to water vapor in a closed chamber for 3 h. As shown in Figure S7 in the Supporting Information, even after this treatment the CA in the charged region is still significantly lower than elsewhere, confirming once again the stability of the trapped charges.

In contrast, for the opposite polarity, only half of the maximum (positive) charge density could be deposited. More importantly, positive charges are unstable (Figure 5c) and relax within a few hours of continuous probing with a water drop in ambient oil. Due to this lack of stability, we did not explore positive charges in more detail.

Figure 5d summarizes these observations: When a relative high voltage is applied in EWOD systems, the charges accumulate at the TPCL region during charging process due to the local wedge shape of liquid and the fringe effect. After tuning off the voltage and taking away the electrolyte droplet, the negative charges are stably trapped in the previous TPCL region with a tunable charge density depending on the charging conditions. In contrast, the positive charges are only temporarily trapped on the polymer surfaces, suggesting that the traps for positive charges are shallower than those for negative ones.

This discussion raises the question about the nature and origin of the trapped surface charge. This question is probably closely related to the long-standing debate about the charge of hydrophobic–water interfaces on the colloidal scale.^[52] Extensive studies (e.g., titration, electrokinetics) have demonstrated that such interfaces preferentially carry negative charge. Based on the widely observed increase with increasing pH, it is believed that the charge density is caused by adsorbing hydroxide ions.^[53–56] Yet, molecular dynamic simulations suggested that hydronium ions adsorb more strongly and sum frequency generation spectroscopy failed to detect the expected OH-stretch vibrations.^[52] The latter leads to theoretical models predicting partial charge transfer. Our current measurements do not provide direct answers to this puzzle. Nevertheless, they do support the stronger affinity of negative charges to the interface, consistent not only with electrokinetics and the earlier report on spontaneous water-aged AFP surfaces,^[31] but also with the better stability of negative charges in corona-charged electrets.^[57] Since we did not intentionally add any salt, the only anions present in our solution should be hydroxide ions. It may well be that these ions donate their excess electron to polymer surface leading to similar trapped electronic states as commonly used to describe corona-charged electret materials. Note, however, the observed charge densities are very low, corresponding to a few hundred square nanometers per unit charge. As a consequence, attempts to detect them spectroscopically by X-ray photoelectron spectroscopy and thus determine their chemical nature have remained elusive.^[58]

2.2.2. Creating Narrow Charge Distributions

According to the classical EW theory,^[34,35] the high electric charge densities should be localized within a region of the order of the thickness of the dielectric layer. These enhanced local electric charge densities and the corresponding electric fields are supposed to be responsible for the charge injection. Following this thought, the intrinsic charge generation mechanism should allow to generate much narrower charge distribution region than the measured width of 200–300 μm . A solution of the electrostatic problem adapted to the parameters of the present experiments shows that the region, in which the local electric field exceeded the average field U_c/d under the

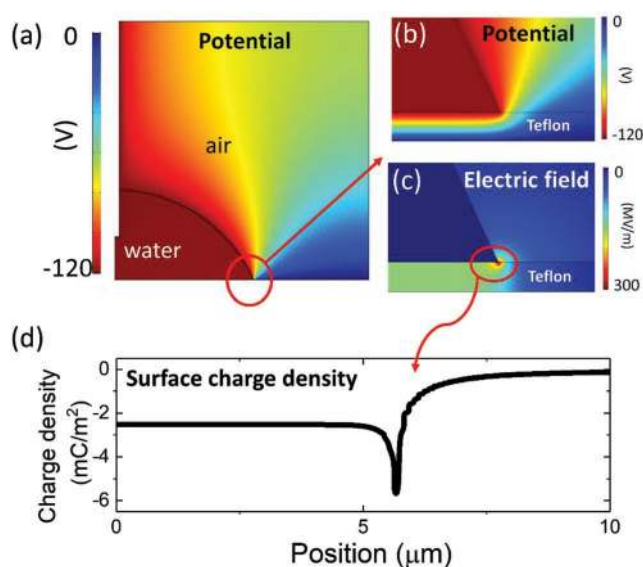


Figure 6. Fringe effect simulation using finite element method (on Comsol platform) a) of the potential of the whole simulation region, b) the potential, c) the electric field, and d) the charge density on the drop near the contact line. For details of the simulations, see the Supporting Information and Figure S8 in the Supporting Information.

charging drop by more than a factor of two, is less than 1 μm in width, as shown in Figure 6. We attribute the wide charge trapping distribution region to the relaxation of the contact line position during the charging process that accompanies the CA relaxation (Figure 1b,c). As it is shown in Figure 1c, the TPCL recedes for $\approx 200 \mu\text{m}$ during charging process and the slowly receding contact line leaves behind a trace of charges on the surface, which eventually forms the observed charge trapping rim. The calculations shown in Figure 6 also indicate the well-known fact that local electric field diverges near the TPCL and is therefore much higher than anywhere at along the electrode/fluoropolymer interface. As a consequence, we assume that charge injection from the bottom electrode is negligible compared to the TPCL region.

In order to reduce the width of the deposited rim of charges, we suppress the geometric relaxation of the drop during charging by confining it between two parallel plates at a distance of $h = 100 \mu\text{m}$ (Figure 7a,b). h is simply achieved by placing a 100 μm thick glass space between the two plates. The lower surface is a Teflon-coated substrate as before and the upper one is an indium tin oxide (ITO)-coated glass that serves as an electrode during the charging process. These two surfaces confine a drop during charging and reduce the displacement of the contact line ΔR for the same amount of CA relaxation $\Delta\theta$ as in Figure 1, with $\Delta R \propto h \Delta(\cos \theta)$. KPFM measurements after removing the top surface and the drop demonstrate that indeed a much narrower rim of charges is deposited with a width of about 20 μm , as shown in Figure 7. The average surface potential within the rim is -10 V , corresponding to the trapped charge density $\sigma_T = -0.22 \text{ mC m}^{-2}$. From these results, we could also conclude that a much smaller but finite charge density is deposited at the solid–liquid interface away from the contact line, as seen in Figure 4. However, the edge of the

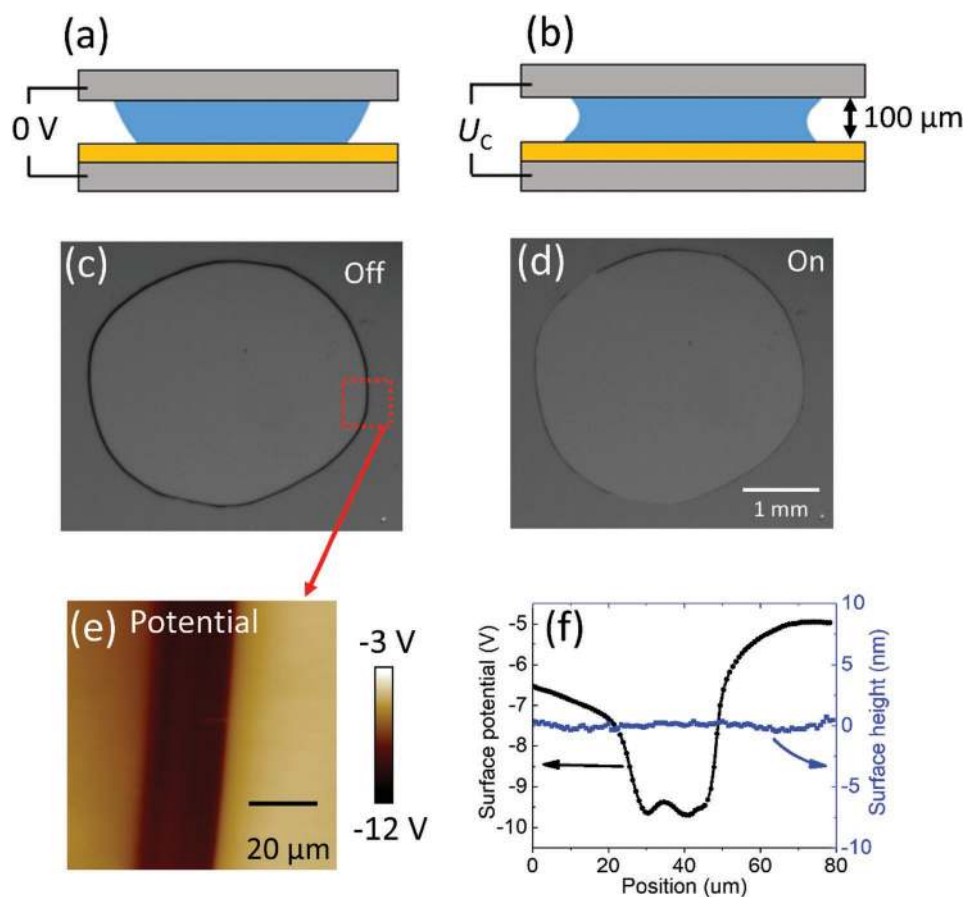


Figure 7. Generation of narrow charge patterns using a confined drop with $U_C = -90$ V for 5 min. a,b) Schematic setup in voltage off and on state. The parts in blue, orange, and gray are water, Teflon AF, and ITO layer, respectively. The thickness of Teflon AF layer is 800 nm. c,d) Corresponding bottom views in transmission illustrating the small variation in radius. e) KPFM surface potential map of the region indicated in (c) after tuning off the voltage and removing the water. f) Line profiles of surface topography and surface potential of charged region in (e).

charged rim is still sharp, suggesting that a further reduction of the width of the rim toward the intrinsic limit should be possible. Thus, by altering the charging voltage, charging time, and controlling the TPCL motion, we demonstrated that EWCI is a promising strategy to produce surface charge distributions with microscale resolution.

There are other approaches to manipulate the TPCL than shown in this work, to meet the requirements of the application at hand. For example, charge injection with a straight boundary can be achieved by dipping the sample partially into a container filled with water resulting in a straight TPCL. It is also conceivable to write a line of surface charge by dragging a small drop or liquid meniscus attached to a microcapillary across a solid surface while applying a voltage, similar to the previous report by Banpurkar et al.^[59] If the applied voltage is varied depending on the position on the surface, EWCI should thus enable the writing of arbitrary charge patterns with a wide range of possible applications (see Figure S9, Supporting Information).

The charge densities generated by EWCI are comparable (or even slightly higher) to conventional charge injection methods such as corona discharge or electron beam

injection. While the lateral resolution of electron beam (or even AFM-based) charge injection is higher,^[60] EWCI allows for reasonably sharp charge patterns on the micrometer scale with minimal equipment requirements. Compared to corona discharge, EWCI is clearly superior both regarding the ability of patterning and regarding the stability of the injected charge, in particular in the presence of humidity.

3. Conclusion

In this work, we conclusively show that, the deposition of surface charges from an aqueous drop on an electrically insulating fluoropolymer surface in an EW configuration at high voltage, indeed preferentially occurs along the contact line of the drop, in accordance with the established EW theory but deviating from recent suggestions based on unconventional and/or unstable EW systems^[27,36,37] in which the maximum charge densities are reported accumulated in the center of the drop. This observation is confirmed by a combination of three experimental techniques, namely, local CA at zero voltage, the asymmetry of the EW response, and KPFM.

Furthermore, we propose this EWCI method as a simple and low-cost strategy for generating surface charges at micro-scale. We demonstrate the tunability of the charge density and the charged regions by simply adjusting the electric charging conditions or confining the motion of TPCL. No vacuum process or other complex facilities are needed. In addition, negative charge patterns are very stable over long times, in dry and humid environment and even in water. We believe that this proposed EWCI strategy will be beneficial for a wide range of research and applications which require controllable surface charges.

4. Experimental Section

Preparation of Teflon Films: ITO/glass substrates were cleaned in a liquid crystal display cleaning line for G2.5 glass (400 mm × 500 mm). Subsequently, 800 nm thick AFP films were prepared by screen-printing Teflon AF 1600 solution with solvent of FC-43 (The Chemours Company, USA), followed by baking on a hot plate at 95 °C for 1 min to remove residual solvent and additional baking in an oven at 185 °C for 30 min to anneal the film. All processes were carried out in a clean room. More details on the fabrication process can be found in ref. [61]. A water drop sliding on the Teflon surface is shown in Video S3 in the Supporting Information.

Surface Charging: Teflon surfaces were charged by applying DC voltages U_C of up to ± 140 V for 2–15 min between the ITO electrodes on the substrate (kept at electrical ground potential) and a platinum (Pt) wire (0.1 mm diameter) immersed into a 5 μL drop of deionized water (MilliQ). Charging the surface was performed at room temperature (≈25 °C) in a closed container filled with vapor-saturated air. Electrical voltages were generated by a function waveform generator (33220A, Agilent, USA) in combination with an amplifier (PZD 700, Trek, USA). The charging voltage U_C was typically chosen within the range of CA saturation, in which θ depends only weakly on the applied voltage (see Figure S1, Supporting Information). U_C was limited to ensure that the simultaneously measured current on the substrate remained below 1 μA for all experiments. Since the current induced by the trapping charges was sub-nA level, the leakage current did not indicate the amount of trapped charges (detailed explanation can be found in the description of Figure S6, Supporting Information)

Surface Characterization—CA Measurements: The wettability of the samples was measured using a commercial CA goniometer (OCA-15+, Data Physics, Germany). Advancing and receding CAs of the Teflon surfaces in air prior to charging were $\theta_a^{\text{air}} = 120^\circ$ and $\theta_r^{\text{air}} = 115^\circ$. All subsequent CA measurements after charging with and without EW were carried out in ambient silicone oil (317667, Sigma-Aldrich, USA) with probe droplets of 0.3–0.5 μL, substantially smaller than the charging drop. All reported voltages were measured with respect to the grounded ITO electrodes. The water drop was in contact with the Pt wire at all time, i.e., CAs at zero voltage corresponding to a configuration with an electrically grounded droplet (i.e., the droplet was not freely floating). The advancing and receding CAs under these conditions were close to 170° with negligible hysteresis. The EW response was probed by applying a triangular waveform (±30 V) with a period of 60 s to the probe drop. The maximum voltage during the EW-surface characterization measurements was kept deliberately low to ensure that the system displayed a parabolic response following Equation (2). In Equation (2), the capacitance per area is $c = \frac{\epsilon_0 \epsilon_r}{d} = 2.2 \times 10^{-5} \text{ F m}^{-2}$. $\gamma = 41 \text{ mJ m}^{-2}$ is the oil–water interfacial tension ($\epsilon_0 \epsilon_r$ and $d \approx 800 \text{ nm}$: dielectric permittivity and thickness of Teflon AF layer). The surface charge densities were calculated with Equation (3) under the assumption that the deposited charge with density σ_T was resided on top of the Teflon surface and did not penetrate substantially into the bulk of the material. Penetration to a depth δ would lead to an enhanced capacitance $c(\delta) = c \cdot d/(d - \delta)$. However, as long as δ was only a few nm, i.e., small

fraction of d , the resulting correction would thus be minor. In addition, a finite charge on the surface automatically implied that $\theta(U = 0) < \theta_Y$. Correspondingly, there was a finite screening charge density $\sigma_D(U = 0) = \sigma_T \frac{c_{\text{EDL}}}{c + c_{\text{EDL}}} \approx \sigma_T$ on the drop ($c_{\text{EDL}} \gg c$: electric double layer capacitance). In contrast, denoted was $\theta_Y = \theta(U_T)$ as Young's angle, which corresponded to the CA of zero charge on the drop. For more detailed aspects of EW measurements including their interpretation in the presence or absence of surface charges, see ref. [6].

KPFM: To characterize the electrostatic potential of the surface in more detail and with high lateral resolution, KPFM measurements were performed using a commercial AFM (Dimension Icon Bruker, USA) with conductive (Sb-(n)doped Si) rectangular tips with a nominal tip radius of 25 nm (SCM-PIT-V2, BRUKER, USA). Upon applying an AC voltage ($U_{\text{AC}} = 500 \text{ mV}$, $f = 60 - 62 \text{ kHz}$) superimposed onto a DC voltage (U_{DC}) to the AFM tip, the electrostatic force (F_{es}) between the AFM tip and sample was given by

$$F_{\text{el}} = \frac{1}{2} \frac{\partial C(z)}{\partial z} (U_{\text{DC}} - U_T + U_{\text{AC}} \sin \omega t)^2 \quad (4)$$

here $\partial C(z)/\partial z$ is the gradient of the capacitance between tip and sample surface and U_T is the trapping voltage. Splitting the force according to their frequency (ω), obtained was the static (F_{DC}) and dynamic (F_ω and $F_{2\omega}$) contributions, as usual

$$F_{\text{DC}} = \frac{\partial C(z)}{\partial z} \left[\frac{1}{2} (U_{\text{DC}} - U_T)^2 + \frac{1}{4} U_{\text{AC}}^2 \right] \quad (5)$$

$$F_\omega = \frac{\partial C(z)}{\partial z} (U_{\text{DC}} - U_T) U_{\text{AC}} \sin \omega t \quad (6)$$

$$F_{2\omega} = -\frac{1}{4} \frac{\partial C(z)}{\partial z} U_{\text{AC}} \cos 2\omega t \quad (7)$$

The amplitude of F_ω was proportional to $U_{\text{DC}} - U_T$. To obtain the U_T in amplitude modulation KPFM, U_{DC} was adjusted such that F_ω became minimal. For a system with a perfectly homogenous dielectric film and a bottom electrode layer, the surface potential U_S was expected to be identical with the trapping voltage U_T . More details on measuring U_T with the KPFM can be found in the Supporting Information and Figure S4 in the Supporting Information.

Supporting Information

Supporting Information is available from the Wiley Online Library or from the author.

Acknowledgements

This work was supported by National Key R&D Program of China (2016YFB0401501), National Natural Science Foundation of China (grant nos. U1501244, U1601651), Program for Chang Jiang Scholars and Innovative Research Teams in Universities (no. IRT_17R40), Science and Technology Project of Shenzhen Municipal Science and Technology Innovation Committee (GQYCCZ20150721150406), Guangdong Provincial Key Laboratory of Optical Information Materials and Technology (no. 2017B030301007), MOE International Laboratory for Optical Information Technologies, Science and Technology Program of Guangzhou (No. 2019050001), and the 111 Project.

Conflict of Interest

The authors declare no conflict of interest.

Keywords

charge trapping, electrets, electrowetting, hydrophobic–water interfaces, surface charges

Received: October 7, 2019

Revised: November 13, 2019

Published online: December 11, 2019

- [1] M. I. B. Utama, H. Kleemann, W. Zhao, C. S. Ong, H. Felipe, D. Y. Qiu, H. Cai, H. Li, R. Kou, S. Zhao, *Nat. Electron.* **2019**, 2, 60.
- [2] H. Cheema, J. H. Delcamp, *Adv. Energy Mater.* **2019**, 9, 1900162.
- [3] H. Wu, L. Wu, X. Zhou, B. Liu, B. Zheng, *Small* **2018**, 14, 1802128.
- [4] H. H. Choi, K. Cho, C. D. Frisbie, H. Sirringhaus, V. Podzorov, *Nat. Mater.* **2018**, 17, 2.
- [5] H. Wu, R. A. Hayes, in *Responsive Polymer Surfaces: Dynamics in Surface Topography* (Eds: D. Liu, D. J. Broer), Wiley, New York **2017**, Ch. 8.
- [6] F. Mugele, J. Heikenfeld, *Electrowetting: Fundamental Principles and Practical Applications*, John Wiley & Sons, New York **2018**.
- [7] D. Baratian, R. Dey, H. Hoek, D. Van Den Ende, F. Mugele, *Phys. Rev. Lett.* **2018**, 120, 214502.
- [8] Y. B. Sawane, S. B. Ogale, A. G. Banpurkar, *ACS Appl. Mater. Interfaces* **2016**, 8, 24049.
- [9] C. E. Clement, S. K. Thio, S.-Y. Park, *Sens. Actuators, B* **2017**, 240, 909.
- [10] F. Mugele, J.-C. Baret, *J. Phys.: Condens. Matter* **2005**, 17, R705.
- [11] H. Wu, R. A. Hayes, F. Li, A. Henzen, L. Shui, G. Zhou, *Displays* **2018**, 53, 47.
- [12] Y. Suzuki, D. Miki, M. Edamoto, M. Honzumi, *J. Micromech. Microeng.* **2010**, 20, 104002.
- [13] H. Li, Z. Guo, S. Kuang, H. Wang, Y. Wang, T. Wu, Z. L. Wang, G. Zhu, *Nano Energy* **2019**, 64, 103913.
- [14] S. Gong, J. Zhang, C. Wang, K. Ren, Z. L. Wang, *Adv. Funct. Mater.* **2019**, 29, 1807618.
- [15] M. G. Pollack, R. B. Fair, A. D. Shenderov, *Appl. Phys. Lett.* **2000**, 77, 1725.
- [16] S. K. Cho, H. J. Moon, C. J. Kim, *J. Microelectromech. Syst.* **2003**, 12, 70.
- [17] B. Berge, J. Peseux, *Eur. Phys. J. E: Soft Matter Biol. Phys.* **2000**, 3, 159.
- [18] K. Mishra, D. van den Ende, F. Mugele, *Micromachines* **2016**, 7, 102.
- [19] R. A. Hayes, B. J. Feenstra, *Nature* **2003**, 425, 383.
- [20] H. Wu, L. Shui, F. Li, R. Hayes, A. Henzen, F. Mugele, G. Zhou, *ACS Appl. Nano Mater.* **2019**, 2, 1018.
- [21] T. Krupenkin, J. A. Taylor, *Nat. Commun.* **2011**, 2, 448.
- [22] H. Wu, H. Li, A. Umar, Y. Wang, G. Zhou, *Materials* **2018**, 11, 2474.
- [23] M. Mibus, X. Hu, C. Knosp, M. L. Reed, G. Zangari, *ACS Appl. Mater. Interfaces* **2016**, 8, 15767.
- [24] B. Raj, M. Dhindsa, N. R. Smith, R. Laughlin, J. Heikenfeld, *Langmuir* **2009**, 25, 12387.
- [25] A. Schultz, S. Chevalliot, S. Kuiper, J. Heikenfeld, *Thin Solid Films* **2013**, 534, 348.
- [26] J. Cao, Q. An, Z. Liu, M. Jin, Z. Yan, W. Lin, L. Chen, P. Li, X. Wang, G. Zhou, *Sens. Actuators, B* **2019**, 291, 470.
- [27] M. Mibus, G. Zangari, *ACS Appl. Mater. Interfaces* **2017**, 9, 42278.
- [28] H. J. J. Verheijen, M. W. J. Prins, *Langmuir* **1999**, 15, 6616.
- [29] D. Thomas, M. C. Audry, R. M. Thibaut, P. Kleimann, F. Chassagneux, M. Maillard, A. Brioude, *Thin Solid Films* **2015**, 590, 224.
- [30] S. Berry, J. Kedzierski, B. Abedian, *Langmuir* **2007**, 23, 12429.
- [31] A. G. Banpurkar, Y. Sawane, S. M. Wadhai, C. U. Murade, I. Siretanu, D. van den Ende, F. Mugele, *Faraday Discuss.* **2017**, 199, 29.
- [32] M. Vallet, M. Vallade, B. Berge, *Eur. Phys. J. B* **1999**, 11, 583.
- [33] K. Adamiak, *Microfluid. Nanofluid.* **2006**, 2, 471.
- [34] J. Buehrle, S. Herminghaus, F. Mugele, *Phys. Rev. Lett.* **2003**, 91, 086101.
- [35] F. Mugele, J. Buehrle, *J. Phys.: Condens. Matter* **2007**, 19, 375112.
- [36] X. M. Li, H. M. Tian, J. Y. Shao, Y. C. Ding, X. L. Chen, L. Wang, B. H. Lu, *Adv. Funct. Mater.* **2016**, 26, 2994.
- [37] M. Mibus, X. Y. Hu, C. Knosp, M. L. Reed, G. Zangari, *ACS Appl. Mater. Interfaces* **2016**, 8, 15767.
- [38] J. Zhong, Q. Zhong, G. Chen, B. Hu, S. Zhao, X. Li, N. Wu, W. Li, H. Yu, J. Zhou, *Energy Environ. Sci.* **2016**, 9, 3085.
- [39] L. Chen, Q. Shi, Y. Sun, T. Nguyen, C. Lee, S. Soh, *Adv. Mater.* **2018**, 30, 1802405.
- [40] X. Gao, A. Omosebi, J. Landon, K. Liu, *Energy Environ. Sci.* **2015**, 8, 897.
- [41] J. Wang, C. Wu, Y. Dai, Z. Zhao, A. Wang, T. Zhang, Z. L. Wang, *Nat. Commun.* **2017**, 8, 88.
- [42] Q. Sun, D. Wang, Y. Li, J. Zhang, S. Ye, J. Cui, L. Chen, Z. Wang, H.-J. Butt, D. Vollmer, *Nat. Mater.* **2019**, 18, 936.
- [43] G. Zhu, Y. Su, P. Bai, J. Chen, Q. Jing, W. Yang, Z. L. Wang, *ACS Nano* **2014**, 8, 6031.
- [44] J. Chen, J. Yang, Z. Li, X. Fan, Y. Zi, Q. Jing, H. Guo, Z. Wen, K. C. Pradel, S. Niu, *ACS Nano* **2015**, 9, 3324.
- [45] M. Yu, D. Lin, H. Feng, Y. Zeng, Y. Tong, X. Lu, *Angew. Chem., Int. Ed.* **2017**, 56, 5454.
- [46] M. Yang, Y. Zhong, J. Ren, X. Zhou, J. Wei, Z. Zhou, *Adv. Energy Mater.* **2015**, 5, 1500550.
- [47] D. Stein, M. Kruihof, C. Dekker, *Phys. Rev. Lett.* **2004**, 93, 035901.
- [48] A. M. Bannunah, D. Vllasaliu, J. Lord, S. Stolnik, *Mol. Pharmaceutics* **2014**, 11, 4363.
- [49] X. Gao, S. Porada, A. Omosebi, K.-L. Liu, P. Biesheuvel, J. Landon, *Water Res.* **2016**, 92, 275.
- [50] X. Zhu, D. Jańczewski, S. Guo, S. S. C. Lee, F. J. Parra Velandia, S. L.-M. Teo, T. He, S. R. Puniredd, G. J. Vancso, *ACS Appl. Mater. Interfaces* **2015**, 7, 852.
- [51] M. Aramesh, O. Shimoni, K. Ostrikov, S. Prawer, J. Cervenka, *Nanoscale* **2015**, 7, 5726.
- [52] N. Agmon, H. J. Bakker, R. K. Campen, R. H. Henchman, P. Pohl, S. Roke, M. Thämer, A. Hassanali, *Chem. Rev.* **2016**, 116, 7642.
- [53] R. Zimmermann, N. Rein, C. Werner, *Phys. Chem. Chem. Phys.* **2009**, 11, 4360.
- [54] J. Lützenkirchen, T. Preočanin, N. Kallay, *Phys. Chem. Chem. Phys.* **2008**, 10, 4946.
- [55] R. Zimmermann, U. Freudenberg, R. Schweiß, D. Küttner, C. Werner, *Curr. Opin. Colloid Interface Sci.* **2010**, 15, 196.
- [56] T. Preočanin, A. Selmani, P. Lindqvist-Reis, F. Heberling, N. Kallay, J. Lützenkirchen, *Colloids Surf., A* **2012**, 412, 120.
- [57] M. Scharnberg, S. Rehders, Ö. Adiyaman, S. Schröder, T. Strunskus, F. Faupel, *Org. Electron.* **2019**, 70, 167.
- [58] E. Yilmaz, H. Sezen, S. Suzer, *Angew. Chem., Int. Ed.* **2012**, 51, 5488.
- [59] D. 't Mannetje, A. Banpurkar, H. Koppelman, M. H. Duits, D. van den Ende, F. Mugele, *Langmuir* **2013**, 29, 9944.
- [60] P. Mesquida, A. Stemmer, *Adv. Mater.* **2001**, 13, 1395.
- [61] H. Wu, B. Tang, R. A. Hayes, Y. Dou, Y. Guo, H. Jiang, G. Zhou, *Materials* **2016**, 9, 707.